

Large Signal Performance of Tweeters, Micro Speakers and Horn Drivers

Wolfgang Klippel, Klippel GmbH, Dresden, Germany, klippel@klippel.de

ABSTRACT

Loudspeaker dedicated to high-frequency signals may also produce significant distortion in the acoustical output. The nonlinearities in motor and suspension can be modelled by equivalent circuits and dynamically measured by system identification technique based voltage and current monitoring. The identified model is the basis for numerical prediction of the large signal performance and reveals the effect of each nonlinearity. The paper uses this technique for the diagnosis of three different drivers, compares measured and predicted distortion, investigates the thermal power compression and discusses the impact on the perceived sound quality.

1. INTRODUCTION

Nonlinearities in woofers have been investigated for a long time and large signal models have been developed which describe the generation of distortion and other nonlinear symptoms at sufficient accuracy [1 – 7]. Since the displacement is high, the variation of force factor $Bl(x)$, stiffness $K_{ms}(x)$ and inductance $L_e(x)$ versus x are the dominant nonlinearities in most woofers. For the measurement of the nonlinear parameters static, incremental dynamic [12] and full dynamic methods [14] have been developed which reveal the causes of the signal distortion directly.

Most of the well established theory can directly be applied to midrange drivers, tweeters and other transducers operated at high-frequencies. However, the higher the resonance the smaller the displacement. It is questionable whether the displacement varying parameters are still the dominant causes of distortion. A high-frequency driver should be much more linear if the voice coil moves a tenth of a mm. However, micro-speakers developed for cellular phones use almost an equal-length configuration between coil height and gap depth which gives maximal sensitivity and power efficiency. Also high-frequency drivers do not use a regular spider or a surround as found in woofers but use the diaphragm itself or single roll as “suspension”. Here minor differences in the geometry might cause significant differences in the large signal performance.

In any case a good model for motor and suspension distortion may help to quantify the contribution from other nonlinearities such as break-up modes on the diaphragm and the air flow in phase-plug interface of horn compression drivers.

These question are discussed in the paper in the following way:

At first a short summary on the established theory and modern measurement and simulation techniques is given. Extensions and modifications are discussed which are necessary to use these tools on high-frequency drivers.

In a second part these techniques are applied to three drivers used in different applications.

Finally open questions and subjects for further research are discussed.

2. BASIC MODELING

If we speak about loudspeaker parameters we have to define the underlying model first.

Loudspeaker models like any other model result from an abstracting process. They give no complete description of the reality but preserve relevant features and reduce the amount of data significantly.

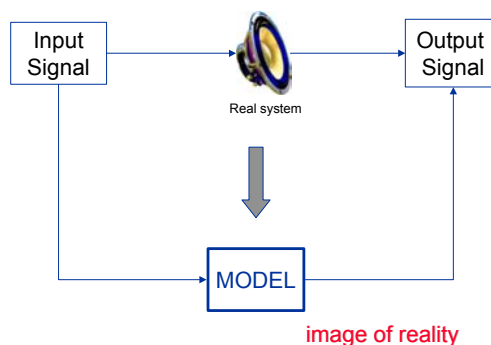


Figure 1: Modeling of loudspeaker systems

There are three different kinds of models important for loudspeaker and other transducers:

- discrete element model
- lumped parameter model
- signal flow chart

These models describe the loudspeaker on different levels of abstraction and will be discussed in greater detail:

2.1. Discrete Element Models

Finite element analysis (FEA) and boundary element analysis (BEA) play an important role in motor and cone design, in the investigation of suspension parts (spiders, surrounds), in describing the radiation and

coupling between mechanical and acoustical vibrations and in modelling the heat transfer [5]. In all these kinds of models the geometry of the parts and the properties of material is considered. This approach preserves a lot of information about the real system but comprises a high number of free parameters.

2.2. Lumped Parameter Model

At sufficiently low frequencies where the wavelength is much larger than the geometrical dimensions of the transducer the state of the loudspeaker can be described by a few number of variables (e.g. current, voltage, displacement, sound pressure in the near field). The relationship between the state variables can be explained by differential equations [3] which may be represented also as an electrical equivalent circuit shown in Figure 2.

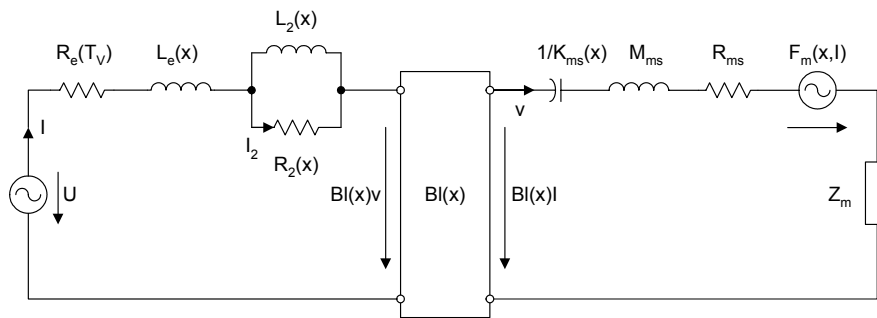


Figure 2: Electrical equivalent circuit of the electro-dynamical transducer

The following time signals are required for describing the instantaneous state:

- $x(t)$ displacement of the voice coil,
- $v(t)$ velocity of the voice coil,
- $i(t)$ the electric input current,
- $u(t)$ the driving voltage at loudspeaker terminals.

The electrical part comprises the following elements:

$R_e(T_v)$	DC resistance of voice coil,	M_{ms}	mechanical mass of driver diaphragm assembly including voice-coil and air load,
$L_e(x)$	part of voice coil inductance which is independent of frequency,	R_{ms}	mechanical resistance of driver suspension losses,
$L_2(x)$	represents the para-inductance of the voice coil,	$K_{ms}(x)$	mechanical stiffness of driver suspension which is the inverse of the compliance $C_{ms}(x)$,
$R_2(x)$	the electric resistance due to additional losses caused by eddy currents,	$F_m(x, I)$	electro-magnetic driving force. due to the variation of the inductance versus x ,
$Bl(x)$	is the effective instantaneous electro-dynamic coupling factor (force factor of the motor) defined by the integral of the permanent magnetic flux density B over voice coil length l .	$Z_m(s)$	mechanical impedance representing mechanical or acoustical load.

The mechanical system is represented by the following elements:

In contrast to the linear model the force factor $Bl(x)$, inductance parameters $L_e(x)$, $L_2(x)$, and $R_2(x)$ and stiffness $K_{ms}(x)$ are constant values but are nonlinear functions of the displacement. However, the nonlinear functions are static which means that there is no frequency dependency in the nonlinearities. Such kinds of nonlinearities can be represented as a nonlinear graph, a table or a power series expansion.

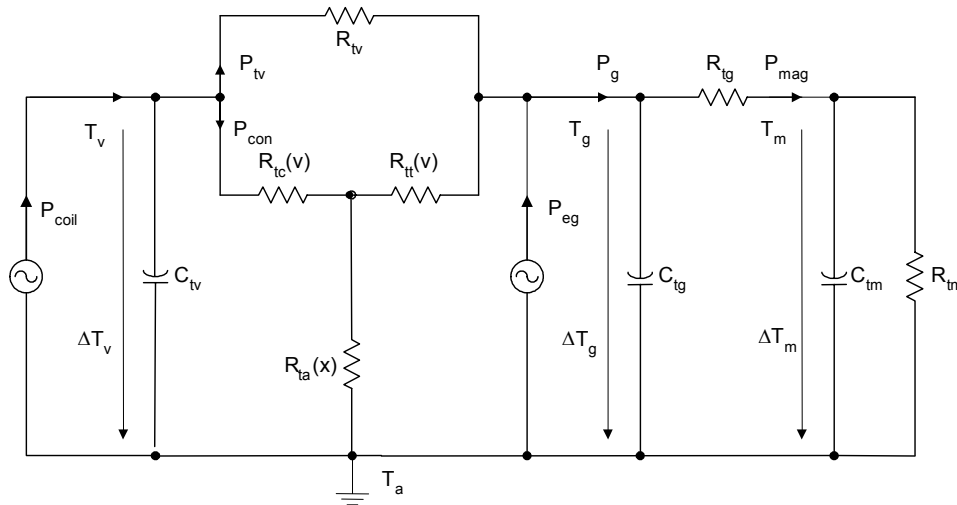


Figure 3: Electrical equivalent circuit to describe the heat flow in the transducer

2.2.1. Thermal Model

The heating of the loudspeaker can also be described by an electrical equivalent circuit [9] as shown in Figure 3.

The thermal state of the transducer is described by the following temperatures and powers which vary with time and depend on the stimulus supplied to the loudspeaker:

T_v	temperature of the voice coil,
T_m	temperature of the magnet structure,
T_g	temperature of the pole tip,
T_a	temperature of the cold transducer (ambient temperature),
$\Delta T_v = T_v - T_a$	increase of voice coil temperature,
$\Delta T_g = T_g - T_a$	increase of temperature of the pole tips,

$\frac{\Delta T_m}{T_a} = T_m -$	increase of the temperature of magnet structure,
P_{coil}	power dissipated in voice coil and former,
P_{eg}	power transferred to the pole tips due to eddy currents,
P_g	power transferred to the pole tips,
P_{iv}	power transferred to the pole tips from coil,
P_{con}	power transferred to the air in the gap due to convection cooling.

The thermal model comprises the following parameters:

R_{iv}	thermal resistance of path from coil to pole tips and magnet surface,
R_{tm}	thermal resistance of path from magnet to ambient air,
R_{tg}	thermal resistance of path from pole tips to magnet and frame,
C_{iv}	thermal capacitance of voice coil and voice coil former (not used for simulation),
C_{tm}	thermal capacitance of magnet and frame (not used for simulation),
C_{tg}	thermal capacitance of pole tips and magnet surface close to coil (not used for simulation),
$R_{ic}(v)$	thermal resistance of path from coil to air in the gap due to convection cooling,
$R_{ia}(x)$	thermal resistance of path from air in the gap to ambience due to convection cooling,
$R_{it}(v)$	thermal resistance of path from air in the gap to the magnet structure due to convection cooling.

The thermal equivalent circuit is a combination of multiple RC-combination giving different time constants for the heating and cooling process of voice coil, pole plates and magnet structure. Both the electro-mechanical and the thermal equivalent circuit are closely interlaced because resistance $R_e(T_v)$ in Figure 2 depends on voice coil temperature T_v and the thermal resistances $R_{ic}(v)$, $R_{ia}(x)$, and $R_{it}(v)$ in Figure 3 depend on displacement x and velocity v of the coil due to the convection cooling.

2.3. Signal flow chart

A signal flow chart is a relatively high abstraction of the reality. It describes the relationship between the input signal (e.g. voltage at the terminals) and internal state

variables (e.g. displacement) and the output signal (e.g. pressure $p(r_i)$ at the listening point r_i in the sound field). The elements of the chart are linear and nonlinear subsystems [11].

The parameter of a linear subsystem is a transfer function $H(s)$ or impulse response $h(t)$ which can be measured by straightforward techniques. The parameters of the nonlinear subsystems require more sophisticated system identification techniques. The signal flow charts are very useful for the assessment of loudspeakers and for the development of special control system to equalize and linearize the transfer behavior.

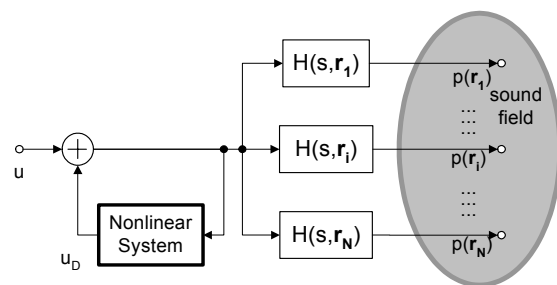


Figure 4: Block model for describing the signal flow between loudspeaker input and sound pressure at listening position

At sufficiently low frequencies, where the lumped parameter model in Figure 2 is valid, the large signal transfer behavior of the loudspeaker can be described by the general signal flow chart shown in Figure 4. The dominant nonlinearities in the motor and suspension can be concentrated in one nonlinear subsystem which generates a distortion signal u_D added to the loudspeaker input signal (e.g. voltage u). The nonlinear subsystem is part of a feedback loop which generates higher-order distortion, compression, bifurcation, instabilities and other complicated interactions between the nonlinearities at higher amplitudes. Whereas the dominant nonlinearities in the motor and suspension are located in the one-dimensional signal path the modeling of the radiation and sound propagation requires a separate linear system with the transfer function $H(s, r_i)$ for each listening point r_i .

The simple model in Figure 4 is the basis for measuring the equivalent input distortion u_D which are independent of the linear properties of the loudspeaker, the room and sensor used.

3. PARAMETER MEASUREMENT

To work with loudspeaker models we have to quantify the free parameters introduced. There is an easy access to the geometrical dimensions required in FEA and

BEA. Material properties (e.g. Young's module and damping parameters) of cone and suspension are also required but more difficult to determine.

The measurement of the linear parameters of the lumped parameter model in Figure 2 can be derived from an impedance measurement of the driver in free air and a second measurement with added mass or in sealed enclosure. However, using a laser displacement sensor dispenses with the time-consuming perturbation technique and gives the mechanical parameters directly. The most important small signal parameters are force factor $Bl(x=0)$ at the rest position and the moving mass M_{ms} . The stiffness K_{ms} of the suspension can not be described by a single number. Also in the small signal domain the stiffness varies with peak displacement, frequency, temperature, humidity and other factors. Due to the visco-elastic behavior of the suspension it is important to measure loudspeakers dynamically by using an audio-like excitation signal and to specify the measurement conditions.

The measurement of the nonlinear and thermal parameters also requires a dynamic technique which is robust, precise and easy to handle.

Since the back EMF generated in an electro-dynamical loudspeaker transfers a mechanical signal (velocity) to the electrical domain we may identify the shape of the transducer nonlinearities by measuring electrical signals (voltage and current at the terminals) only. This task can be solved by a system identification technique [14] as shown in Figure 5 using a time-discrete (digital) model and an adaptive parameter estimator.

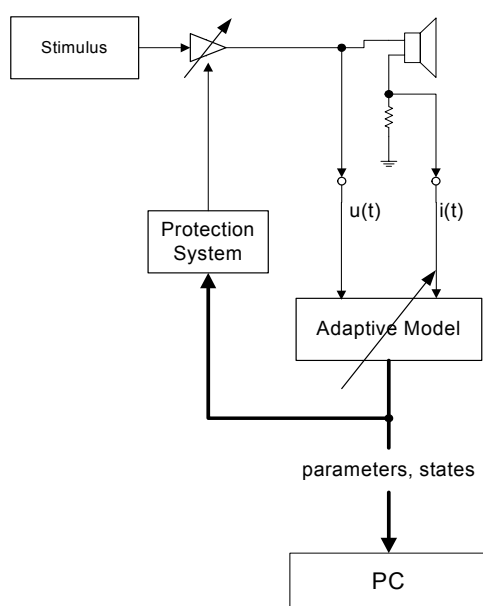


Figure 5: Large signal identification (LSI) of loudspeaker parameters and state variables

This kind of measurement can be used with any audio-like signal giving sufficient excitation of the loudspeaker. A protection system finds the limits of the working range automatically by monitoring nonlinear parameter variation (decay of $Bl(x)$ and compliance $C_{ms}(x)$) and voice coil temperature.

The parameters of the thermal model in Figure 3 are measured in a special mode where the transducer is excited by a sequence of differently shaped noise signals to monitor the heating and cooling process. The large signal identification provides not only loudspeaker parameters (linear, nonlinear, thermal) but also state variables (displacement, voltage, current, ...). The state variables vary in a complicated (nonlinear) way with the stimulus while parameters should be almost independent of the stimulus. Of course ageing, visco-elastic behavior of the suspension and other mechanisms may cause slow variation of the parameters. The peak and rms-value of interesting state variables is measured periodically and stored in a buffer giving a full history of the identification process. Finally the model implemented in a DSP allows to separate the nonlinear distortion generated by force factor, compliance and inductance from the linear signal and to perform a distortion analysis on-line while reproducing music or test signals.

4. MEASUREMENT OF SYMPTOMS

The traditional way of assessing the nonlinear behavior of loudspeakers uses a special test signal. Current standards (IEC) recommend a single-tone or two-tone stimulus combined with a spectral analysis of the output signal to separate the fundamental, harmonic and intermodulation components of different orders.

The measurement of the dc-component in the voice coil displacement is also a sensitive indicator for asymmetries in the loudspeaker nonlinearities [4]. For example a suspension with an asymmetrical stiffness characteristic will dynamically generate a dc force which moves the suspension to the softer side. A coil offset corresponding with an asymmetric force factor characteristic also generates a dc force. The direction of the dc force depends on the frequency of the stimulus. For tones below resonance the coil moves towards the Bl -maximum (self-centering) while for tones above resonance the coil will slide down the $Bl(x)$ -characteristic leading to the coil-jump-out effect.

Tests with a single or two-tones are very useful to investigate the effect of the loudspeaker nonlinearities ($Bl(x)$, $Kms(x)$, ...) and defects (rub & buzz)

systematically. However, a series of single-tone measurement with varied excitation frequency can not describe the nonlinear loudspeaker behavior completely.

Increasing the number of excitation tones while keeping a sparse spectrum (some frequencies are not excited) leads to the multi-tone distortion measurement [15]. This stimulus excites all kinds of harmonic and intermodulation components (like in a real audio signal) which are summarized to an integral distortion measure. This technique provides meaningful “fingerprints” of the large signal behavior in a short time.

All kinds of distortion measurements reveal only symptoms of the nonlinearities but not the physical causes. The relationship between spectral properties of the stimulus, type of nonlinearity and analysis of the monitored signal is important to produce characteristic symptoms. For example a sinusoidal sweep may be a good stimulus for end-of line testing. The analysis of higher-order harmonics in the measured sound pressure

signal may reveal a rubbing coil or other defects. Total harmonic distortion measured with a single tone stimulus at the resonance frequency is also a good indicator for stiffness nonlinearity $K_{ms}(x)$ but not for inductance nonlinearities which require a two-tone and multi-tone stimulus. A particular test signal which satisfies all demands is not known.

Performing nonlinear distortion measurements at many points in the sound field are neither feasible nor useful in practice. A large amount of redundant data is produced which is hard to interpret. However, the effect of the motor and suspension nonlinearities as modeled in Figure 2 can be assessed at one-point which is preferably located in the near field where the signal-to-noise ratio is high. The distortion measured at this point may be transformed into equivalent input distortion u_D as shown in Figure 4. The inverse filtering compensates for the influence of the linear transfer response and simplifies the interpretation of the distortion responses.

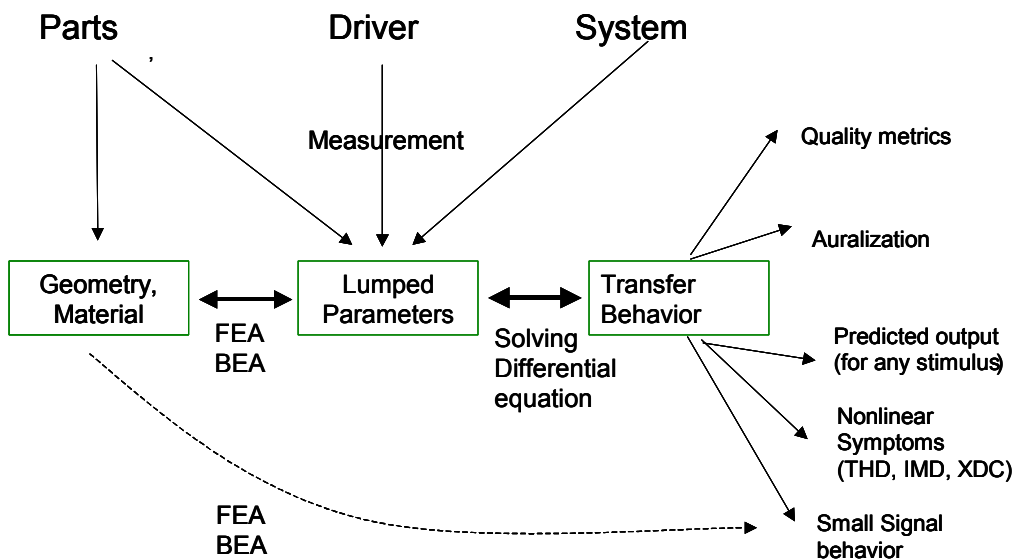


Figure 6: Loudspeaker diagnostics

5. DIAGNOSTICS

The development of loudspeakers which are optimal with respect to performance, cost, weight and size requires knowledge how the geometry and material of the parts influence the final loudspeaker performance. The relationship is very complex as illustrated in Figure 6. A tool which predicts the relationship between design and quality metrics (e.g. sound quality perceived by the listener or preference by a customer) has not been

developed yet. Currently FEA and BEA may be used to predict the linear transfer response for a certain geometry and material properties. The linear transfer response may be convoluted by an audio signal to predict the loudspeaker output at small amplitudes and applied to subjective testing. Unfortunately, this approach is limited to the small signal domain. FEA and BEA considering only the most important loudspeaker nonlinearities and applied to normal test signals or music requires significant calculations which can not be solved by available processors in reasonable time [5]. It is also very questionable whether such a “black box”

would be very helpful for the loudspeaker design. The current way of investigating the motor structure (coil in magnetic field) separately from the break-up modes on cone and independently of the thermal behavior keeps the complexity manageable and allows to use efficient numerical tools dedicated for the particular problem. The result of motor design may be a electrical impedance of the voice coil (versus frequency and depending on displacement and current) and the force factor characteristic (versus displacement). An FEA applied to a suspension may result in a nonlinear stiffness characteristic $K_{ms}(x)$ and the creep factor λ to describe the visco-elastic behavior. The result of an FEA of a diaphragm coupled with a BEA of the

acoustical environment may be a linear transfer function between driving force of the voice coil and the sound pressure at the listening position. An FEA applied to the heat flow may produce the thermal parameters of the loudspeaker.

The linear, nonlinear and thermal parameters calculated by FEA/BEA can be compared with parameters directly measured on a real loudspeaker (e.g. LSI). Finally the overall transfer behavior can be predicted for any input signal by solving the lumped parameter model [17] while considering dominant nonlinear and thermal effects.

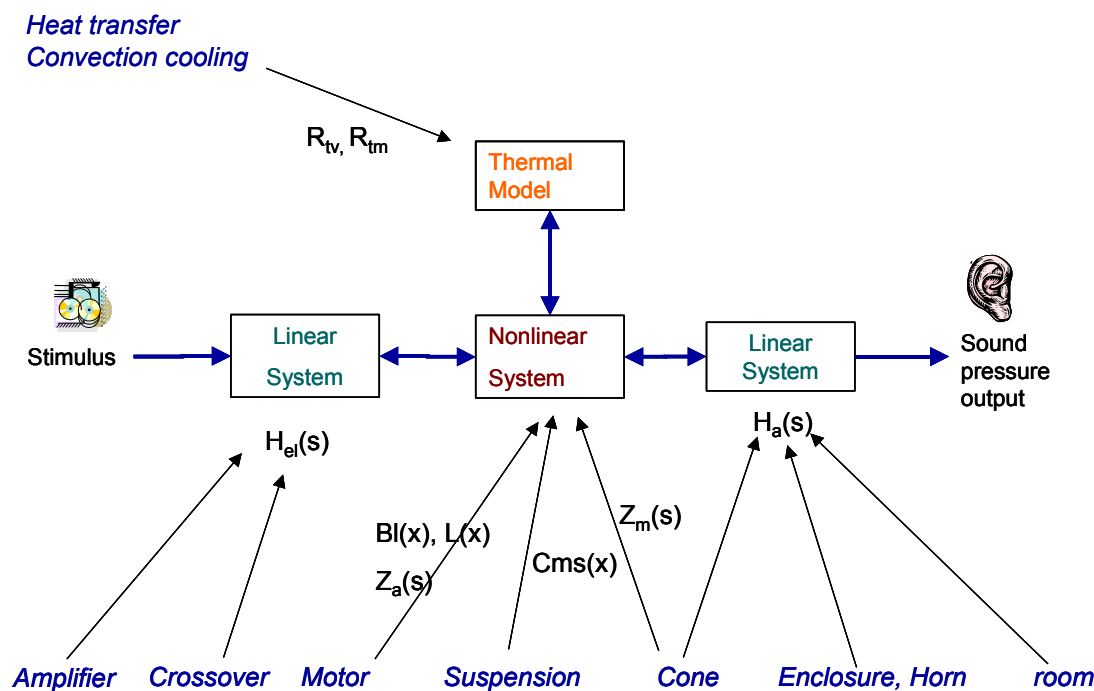


Figure 7: Prediction of the transfer behavior on the basis of a lumped parameter model

Figure 7 shows a first implementation of this approach in the Large Signal Simulation Module (SIM) [18]. It comprises a sandwich structure where a nonlinear kernel is embedded by two linear systems. The first linear system $H_{el}(s)$ represents the effect of an amplifier or an active or passive crossover. The nonlinear kernel solves the nonlinear differential equation by numerical integration considering the dominant nonlinearities in driver and enclosure, the heat flow and the impedance

$Z_m(s)$ of the coupled mechanical or acoustical system. Finally a second linear system $H_a(s)$ models the radiation and propagation in the sound field. This tool calculates all relevant state variables (displacement, current, volume velocity in port, sound pressure, ...) for a two-tone excitation signal. An FFT analysis reveals relevant symptoms such as dc displacement X_{DC} , fundamental and distortion components in a very short time. The results can easily be compared with directly

measured symptoms to verify the modeling. If a model of the loudspeaker is established the effect of each nonlinearity can be investigated systematically by changing the shape of the nonlinearities or switching off some of the nonlinearities.

6. DISCUSSION OF EXAMPLES

The loudspeaker diagnostic shall be illustrated on some practical examples:

- conventional tweeter with ceramic magnet for multi-channel loudspeaker system
- horn compression driver intended for professional application.
- micro-speaker used in cellular phones

6.1. Tweeter

The small signal parameters have been identified from voltage, current and displacement using the module Linear Parameter Measurement (LPM) and a laser displacement sensor.

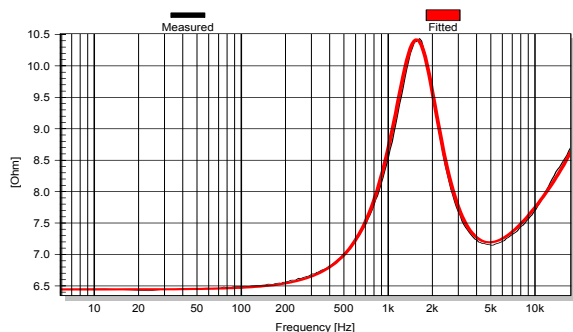


Figure 8: Magnitude of electrical input impedance $Z(s)=U(s)/I(s)$ of a tweeter versus frequency

Figure 8 shows a good agreement between the measured impedance response (thin line) and the fitted response (thick line). The resonance frequency is about 1.5 kHz and a relatively low total loss factor of $Q_{ts} = 0.83$ was found in the small signal domain where the electrical loss factor $Q_{es}=2$ was dominated by the mechanical loss factor $Q_{ms} = 1.42$.

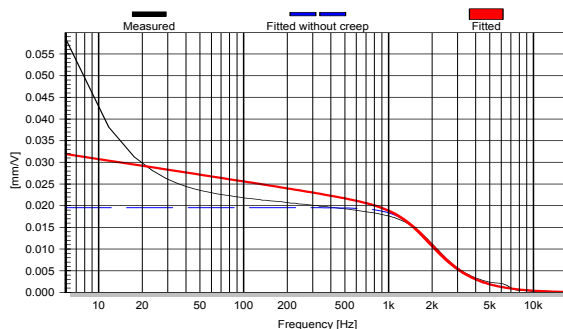


Figure 9: Magnitude response of mechanical transfer function $H_x(s)=X(s)/U(s)$ of the tweeter

The transfer function $H_x(s)=X(s)/U(s)$ in Figure 9 describes the relationship between voltage u and voice coil displacement x . The measured displacement (thin solid line) increases at low frequencies contrary to the dashed line staying constant at low frequencies as expected in the classical model shown in Figure 2. The difference is caused by visco-elastic behavior of the suspension and magneto fluid in the gap and may be modeled by a frequency depending compliance as suggested by Knudsen [13] and shown as thick solid line in Figure 19. This model uses a creep factor of $\lambda=20\%$ meaning that the compliance increases by 20 % for a frequency one decade below resonance. A low creep factor preserves maximal stiffness at very low frequencies which gives minimal dc displacement for any given asymmetries in the loudspeaker nonlinearities.

The large signal parameters have been identified by a new large signal identification module (LSI Tweeter) dedicated for transducers with a high resonance frequency. The tweeter was clamped in free air and excited by a white noise signal low-pass filtered at 1.5 kHz to excite the tweeter to large displacement while keeping the voice coil temperature low.

The large signal identification started in the small signal domain with an input voltage of 400 mV rms giving 0.05 mm peak displacement only. At the beginning the resonance frequency, and the loss factors detected by the adaptive model in the LSI module were almost identical with the LPM measurement using a multi-tone stimulus. However, with the increase of the voice coil temperature ($\Delta T_v = 40\text{ K}$) the electrical loss factor Q_{es} rose slowly from 2.1 to 2.55. More important is that some of the mechanical losses disappeared during the 20 minutes LSI measurement giving a final loss factor of $Q_{ms} = 4.4$. This is caused by visco-elastic properties of the magneto-fluid which depends on temperature, exposure to vibration and other unknown variables. Thus, in long term usage of the tweeter the total loss

factor Q_{fs} increases to 1.7 dominated by the electrical damping.

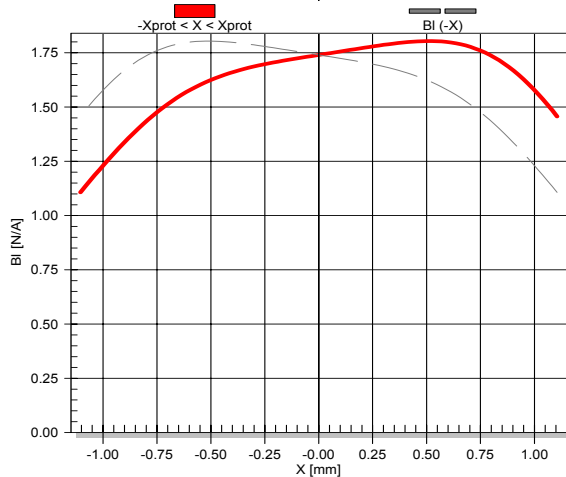


Figure 10: Force factor $Bl(x)$ versus displacement of the tweeter.

The force factor $Bl(x)$ shown in Figure 10 reveals an asymmetry superimposed with a symmetrical decay starting at ± 0.6 mm where the coil leaves the air gap.

The asymmetry is most likely caused by an asymmetrical B -field and can not be compensated by shifting the coil in the gap. During the LSI measurement the $Bl(x)$ -distortion stayed below 15 % of the peak value in the total sound pressure output signal. Force factor variations generate high harmonic distortion up to the resonance frequency (1500 Hz) and broad band intermodulation for any input signal as long as the voice coil displacement is high. In contrast to woofer systems where such intermodulation can easily be detected by an unpleasant roughness of a modulated voice or flute signal the force factor distortion in tweeters is perceived as additional disturbances impairing the clearness of the sound.

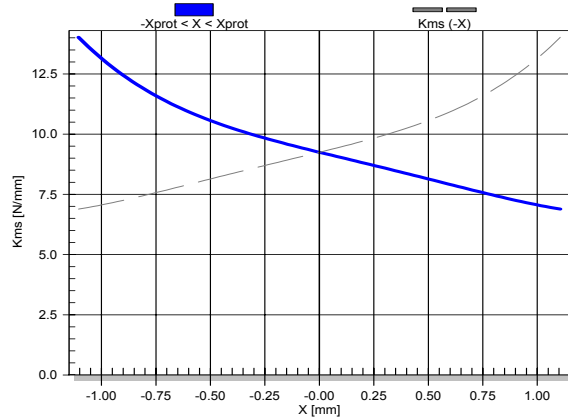


Figure 11: Stiffness $K_{ms}(x)$ versus displacement of the tweeter

Figure 11 reveals a significant asymmetry in the nonlinear stiffness $K_{ms}(x)$ of the suspension. It is caused by the geometry of the outer roll used as suspension. Contrary to most woofers there is no increase of stiffness at positive displacement. The asymmetry contributes to the 2nd-order harmonics for frequencies below resonance. During the LSI measurement the peak value of stiffness distortion exceeded 40 %. Whereas stiffness distortion generated in woofers contains low frequency components only and is perceived as a harder and louder bass sound, the stiffness distortion of a tweeter sounds very similar to $Bl(x)$ -distortion. The asymmetry also generates a dc-force which moves the coil in positive direction.

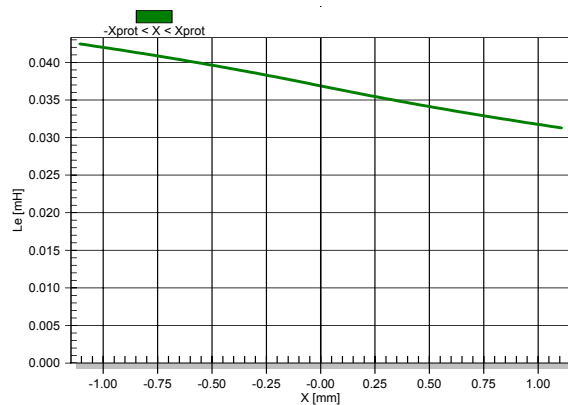


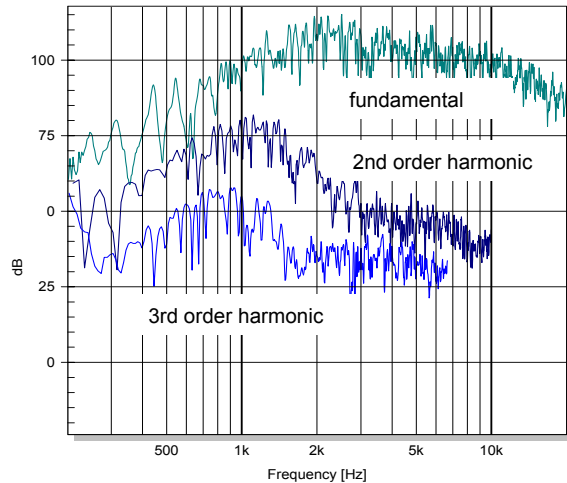
Figure 12: Inductance $L_e(x)$ versus displacement of the tweeter

The inductance characteristic has a shape which is typical for most drivers using no shorting rings or other conductive material (copper caps, aluminium) to reduce the energy in the magnetic ac-field. The nonlinear inductance causes variation of the electrical input

impedance and generates distortion primarily in the input current. The distortion depends not only on the shape of the $L_e(x)$ -characteristic but also on the resistance R_e and the frequency. The stimulus in the LSI measurement generated low inductance distortion (below 2 %).

Large Signal behavior

The total harmonic distortion response is also simulated by using the identified nonlinear parameters and the measured linear transfer response. Figure 14 shows a good agreement between measured (dashed) and predicted (solid) curve. The total harmonic distortion are high at low frequencies where acoustical resonances cause dips in the linear response.



(after 20 min)Figure 13: Fundamental, 2nd-order and 3rd-order harmonic distortion measured in sound pressure output of the tweeter.

Figure 13 shows the fundamental, 2nd- and 3rd-order harmonic distortion measured in the near field of the tweeter. As expected from the shape of the nonlinear parameters the 2nd-order distortion is dominant.

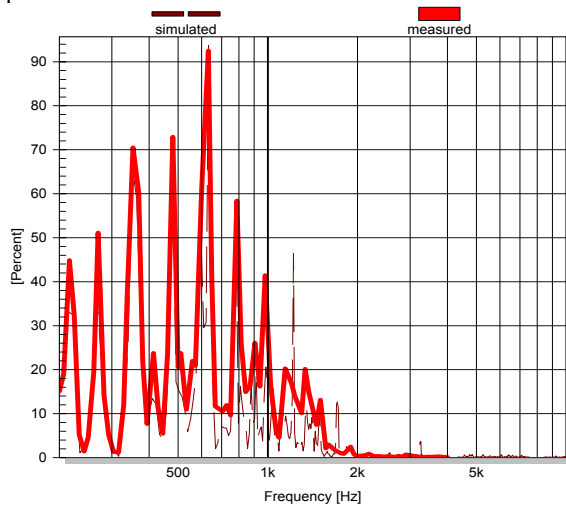


Figure 14: Total harmonic distortion (THD) in measured in sound pressure output (solid line) and predicted by using large signal parameters (dashed line).

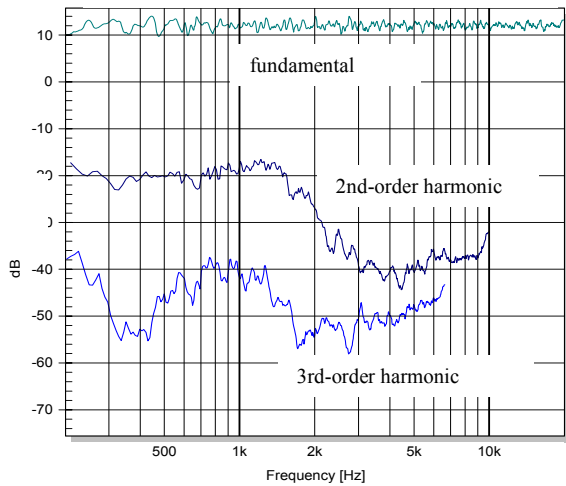


Figure 15: Measured equivalent harmonic input distortion of the tweeter

The influence of the acoustical environment can be removed by performing a filtering of the measured sound pressure signal with the inverse transfer function prior to the spectral analysis. The resulting equivalent harmonic input distortion responses are shown in Figure 15.

Clearly the fundamental response stays flat at 12 dB which corresponds with 4 V rms excitation signal. The 2nd-order distortion is almost constant at -20 dB (0.1 V rms equivalent input voltage) up to 1.5 kHz. The 3rd-order response stayed below 10 mV. There is an additional dip at 400 Hz caused by an interference between the $Bl(x)$ and $K_{ms}(x)$ distortion. However, a compensation of the effects of $Bl(x)$ -nonlinearity by a matched shape of the $K_{ms}(x)$ -nonlinearity is not possible over a wide frequency range.

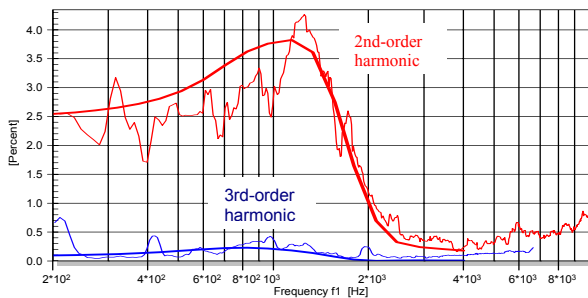


Figure 16: Equivalent harmonic input distortion of the tweeter based on measurement (thin lines) and prediction using large signal parameters (thick lines).

It is also convenient to refer the 2nd- and 3rd-order equivalent input harmonics to the (constant) fundamental voltage (here 4 Volt rms) and to present the distortion ratio in percent as shown in Figure 16.

The thin lines are derived from sound pressure measurements while the thick lines represent the predicted equivalent distortion which are calculated by using the large signal parameter in the SIM module.

The agreement between predicted and measured distortion is good. The minor disagreement at the resonance frequency is caused by the variation of the mechanical damping depending on the length of the measurement.

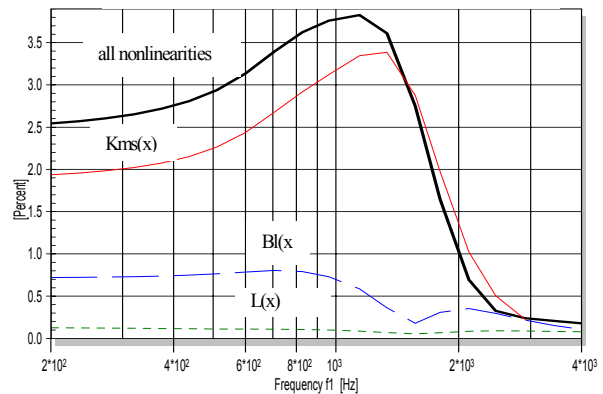


Figure 17: Contribution to the 2nd-order harmonic distortion from nonlinear stiffness (thin line), force factor (dashed line) and inductance (dotted line).

The large signal simulation module (SIM) allows to investigate the effect of each nonlinearity separately. Figure 17 shows that the nonlinear stiffness dominates the 2nd-order distortion. A finite element analysis of the outer zone of the dome would give further insight into the geometrical cause of the nonlinearity.

6.2. Horn Compression Driver

The next example is a horn compression driver using phenolic impregnated fabric as diaphragm and a coil with 51 mm diameter and 4.6 mm height in a 4 mm gap. The horn and the phase plug interface were removed and the rear volume was carefully sealed to avoid any additional acoustical resonance.

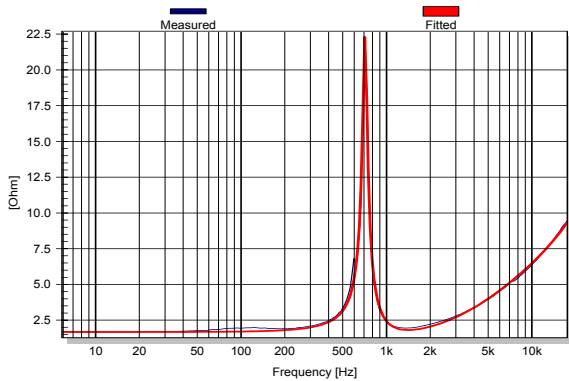


Figure 18: Measured and fitted magnitude response of electrical input impedance of the horn compression driver.

The good fitting of the impedance response in Figure 18 shows that the equivalent circuit in Figure 2 can be applied successfully and the additional mechanical impedance $Z_m(s)$ can be neglected. The driver has a resonance at 728 Hz with relatively low mechanical losses ($Q_{ms}=16$) dominated by the electrical damping giving a total loss factor of $Q_{ts}=1.2$.

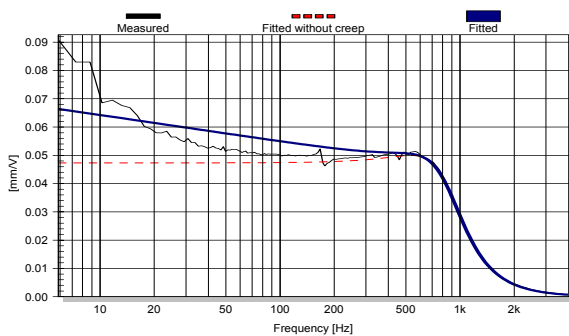


Figure 19: Magnitude of transfer function $H_x(s)=X(s)/U(s)$ versus frequency of the horn compression driver

Figure 19 shows the measured transfer response between voltage and displacement as thin line and the

modeled responses without and with creep model as thick and dotted line respectively. Like the tweeter discussed before the impregnated fabric “forgets” 20 % of the stiffness one decade below resonance.

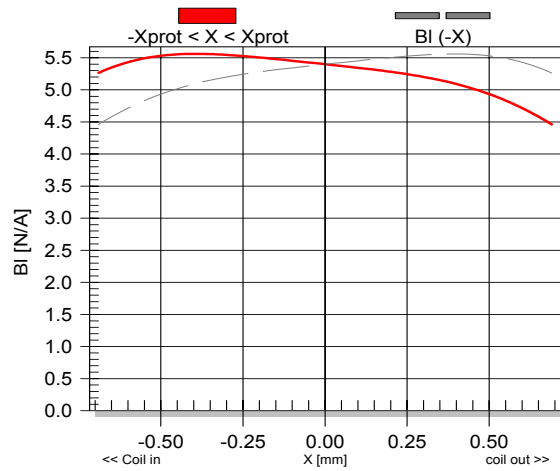


Figure 20: Force factor $Bl(x)$ versus displacement of the horn driver.

The measured force factor characteristic has a distinct asymmetry at small and medium amplitudes which is caused by the B field in the gap. The coil leaves the gap symmetrically at $x=\pm 0.5$ mm. In the investigated working range the $Bl(x)$ -nonlinearity generates more 2nd than 3rd-order distortion. During the LSI measurement the peak value of the predicted $Bl(x)$ -distortion where about 20 % of the peak value of the total sound pressure signal.

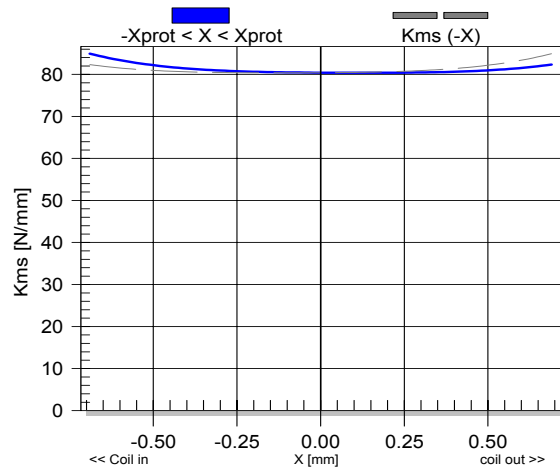


Figure 21: Stiffness $K_{ms}(x)$ versus displacement of the horn driver

The stiffness $K_{ms}(x)$ of the suspension as shown in Figure 21 is almost constant in the investigated working range generating only 5 % distortion in the white noise signal used in the LSI measurement.

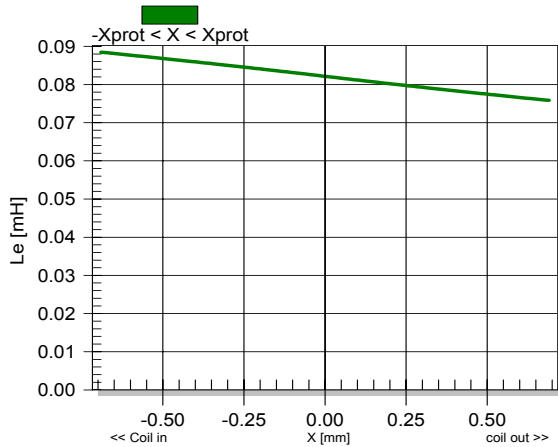


Figure 22: Inductance $L_e(x)$ versus displacement of the horn driver

The inductance in Figure 22 increases with negative displacement which is typical for a motor using no shorting rings. This may cause some 2nd-order intermodulation distortion between a low and high frequency tone which are generated primarily in the input current and found in the same percentage in the sound pressure output. During the LSI measurement $L_e(x)$ -distortion stayed below 5 % of the total sound pressure output.

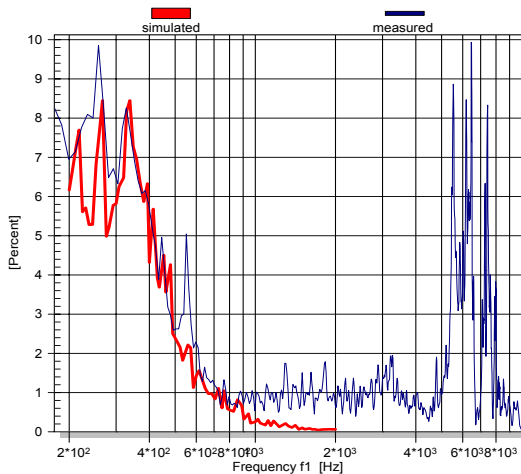


Figure 23: Total harmonic distortion measured in sound pressure output (thin line) and calculated by using the large signal parameters (thick line)

Figure 23 shows the total harmonic distortion predicted from the large signal parameters as thick line. At low frequencies there is a good agreement with the measured distortion displayed as thin line. However, the discrepancy at 8 kHz shows that there are additional nonlinear mechanisms outside the motor which can not be explained by the equivalent circuit in Figure 2.

In order to investigate the cause of the nonlinear distortion at higher frequencies the acceleration of the dome was measured at four different spots equally spaced from the centre to the outer rim. Using a special stimulus pre-shaped with an emphasis of 12dB per octave as provided in the Transfer Function Module (TRF) [18] the acceleration can be measured up to 10 kHz by an inexpensive displacement sensor based on the triangulation principle with sufficient signal to noise ratio.

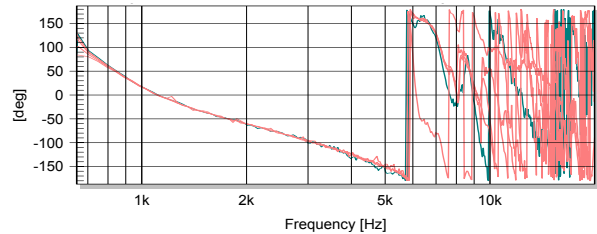


Figure 24: Phase of acceleration measured at four different spots on the dome of the horn driver

The phase in Figure 24 shows that the all four spots vibrate in-phase up to 6 kHz. From 6 to 7.5 kHz the outer rim zone vibrates in anti-phase to the centre part. Above 8 kHz there are more and more break-up modes vibrating in different phases.

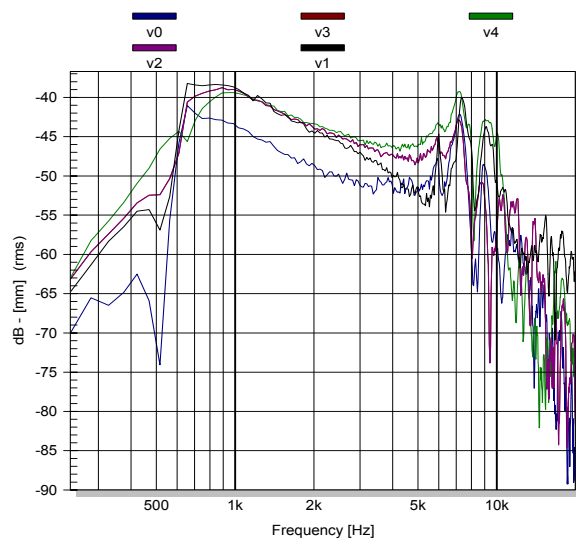


Figure 25: Magnitude of acceleration measured at four different spots on the dome of the horn driver

The magnitude of the acceleration as shown in Figure 25 gradually decreases from the resonance frequency (700 Hz) up to 5 kHz where the first break up mode starts. At 7 and 9 kHz there are distinct maximums at all four spots on the diaphragm corresponding with high total harmonic distortion as shown in Figure 23. There is also a distinct minimum in the magnitude response at 8.5 kHz causing a dip in the fundamental and consequently a peak in the total harmonic distortion. A nonlinear FEA would give deeper insight into the cause of the distortion.

All nonlinearities of the horn driver are relatively small and did not limit the working range of the horn compression driver. However, the heating of the voice coil limited the maximal input power during the LSI measurement.

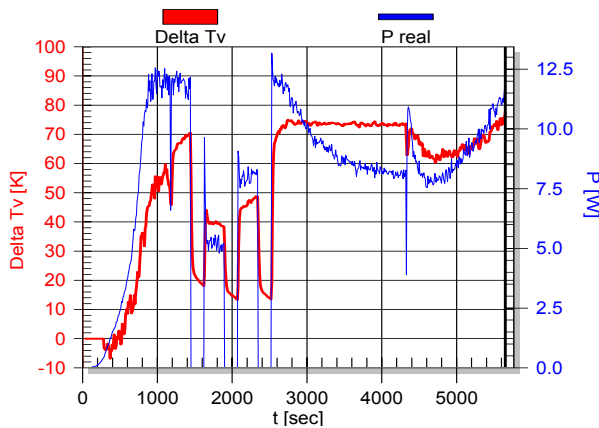


Figure 26: Voice coil temperature T_{tv} (thick curve) and real input power P_{real} versus measurement time

Figure 26 shows the voice coil temperature and the real power dissipated in the horn driver during the LSI measurement. The spectral properties of the stimulus are changed to investigate convection cooling and direct heat transfer to the pole tips due to eddy currents. The horn compression driver could handle up to 12 W real input power while keeping the increase of voice coil temperature below 80 Kelvin.

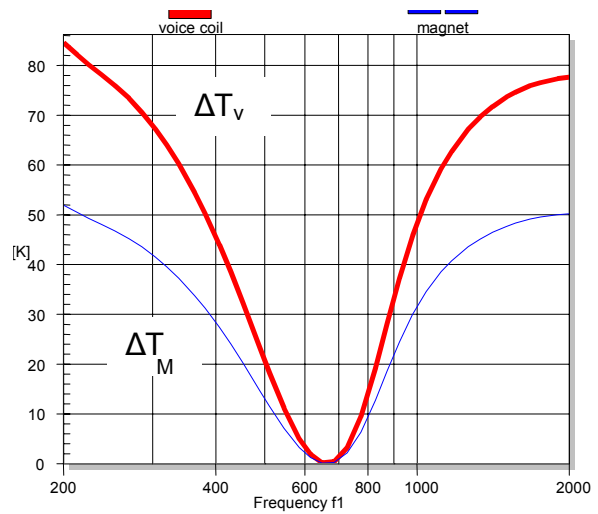


Figure 27: Steady state temperature of voice coil and magnet versus frequency of a sinusoidal stimulus

The identified thermal parameters allow an investigation of the heat flow in greater detail. Figure 27 shows the temperature ΔT_v and ΔT_m of the coil and magnet, respectively, for a sinusoidal input of 4 V rms under steady-state condition. Clearly at the resonance where the impedance is high and the input current is low the temperature becomes small. The high thermal resistance R_{tm} between magnet and environment causes a high magnet temperature ΔT_m . Additional cooling surface mounted to the magnet would improve the power handling of the horn driver.

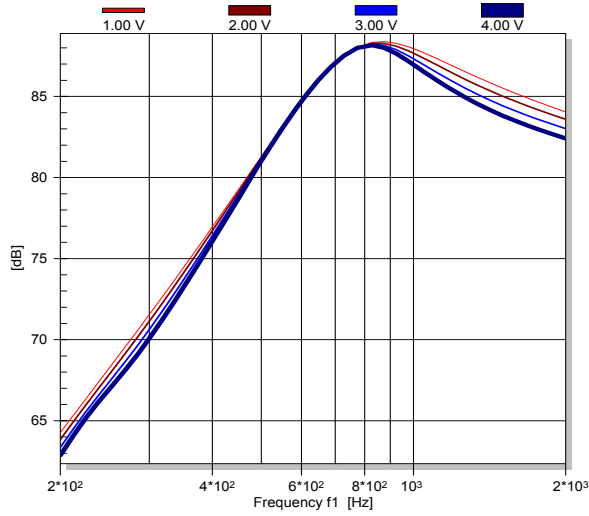


Figure 28: Normalized sound pressure response measured at 1, 2, 3 and 4 Volt of the horn driver to visualize thermal power compression.

The heating of the coil does not only expose the driver to a possible damage but also reduces the sensitivity of the driver. Figure 28 shows the sound pressure responses simulated at four different voltages (1 V increment) but normalized to the first measurement using 1 V rms. This shows the thermal power compression which is about 3 dB for excitation tones below and above resonance.

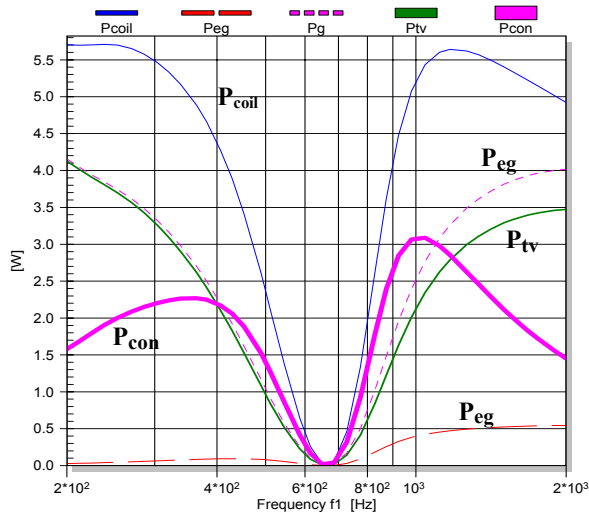


Figure 29: Power flow in the horn driver

The thermal equivalent model implemented in the SIM module allows to investigate the power flow in the horn driver. The power P_{coil} is dissipated in the voice coil but a substantial part P_{con} directly bypasses the coil due to convection cooling but only the power P_{tv} contributes to

the heating of the coil. The convection cooling is only active at frequencies where the velocity is high. At high frequencies the eddy currents in the pole tips are a second mechanism where the power P_{eg} bypasses the coil and only heats the magnet.

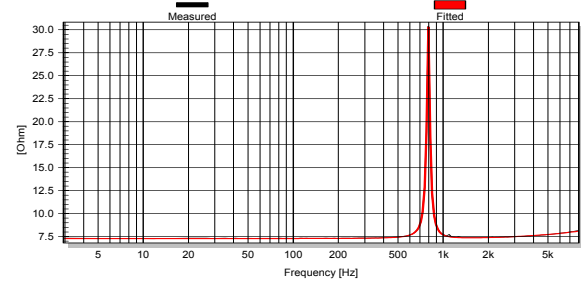


Figure 30: Measured and fitted magnitude of electrical input impedance $Z(f)=U(f)/I(f)$ versus frequency of the micro speaker.

6.3. Micro Speaker

Figure 30 shows the electrical impedance of a micro speaker (9 mm coil diameter) measured in free air. The driver has a resonance frequency at 800 Hz with low mechanical damping ($Q_{ms}=18$) giving a total loss factor $Q_{ts}=5$ which is dominated by the electrical damping ($Q_{es}=7$).

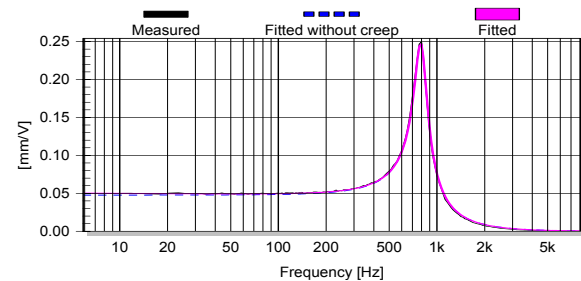


Figure 31: Magnitude response of mechanical transfer function $H_x(s)=X(s)/U(s)$ of the micro speaker.

The synthetic material used for diaphragm and “suspension” has not the typical visco-elastic behavior of impregnated paper and fabric but preserves the stiffness found at resonance also at low frequencies. ($\lambda=2\%$). Thus the classical equivalent circuit without creep model fits perfectly to the measured displacement transfer function displayed in Figure 31.

The large signal identification has been performed by using a white noise stimulus which is band-pass filtered from 150–1500 Hz. The maximal input power was limited to 200 mW giving a maximal peak displacement

of 0.3 mm and an increase of the voice coil temperature by 40 K .

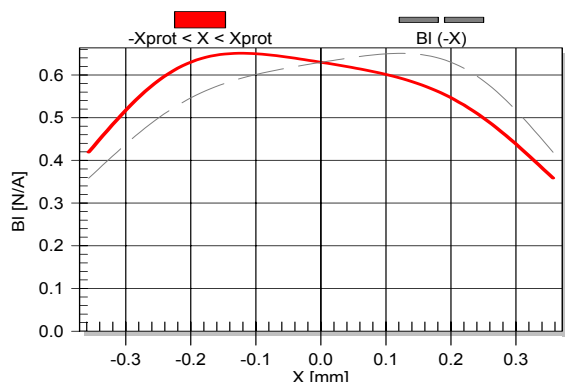


Figure 32: Force factor $BI(x)$ versus displacement of the micro speaker

The force factor reveals a minor asymmetry most likely caused by the B-field but the symmetrical decay starting at 0.2 mm displacement shows that the rest position of the coil is correct.

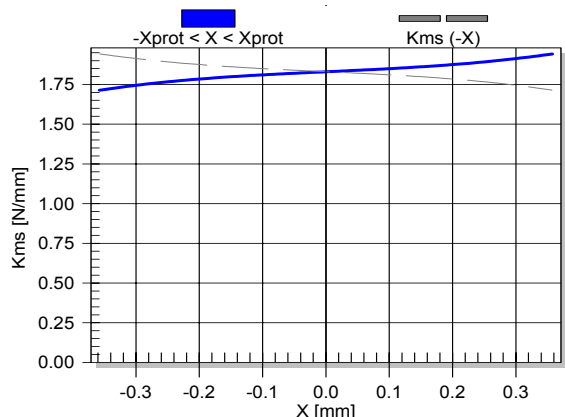


Figure 33: Stiffness $K_{ms}(x)$ versus displacement of the micro speaker

Figure 33 reveals an asymmetric stiffness characteristic. There is no symmetrical increase in the measured working range as found in most woofer systems giving low natural protection the voice coil at high amplitudes.

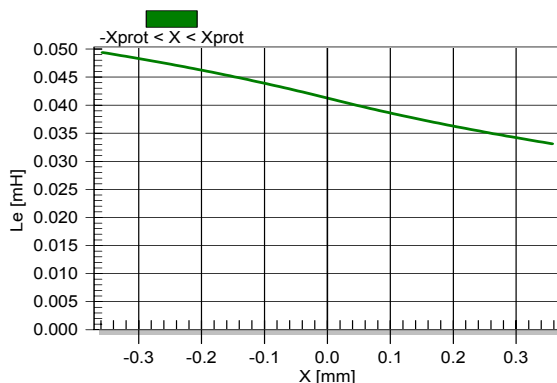


Figure 34: Inductance $L_e(x)$ versus displacement of the micro speaker

The inductance of the coil is very small causing only a minor increase of the impedance in Figure 30. Thus the small asymmetrical variation of the inductance versus displacement as shown in Figure 34 caused only small nonlinear distortion. During the LSI measurement where the filtered white noise signal generated 0.3 mm peak displacement the $L_e(x)$ -nonlinearity only contributed 4 % while the $BI(x)$ contributed 20 % and the stiffness characteristic 10 % distortion to the sound pressure output.

7. CONCLUSIONS

The classical large signal model developed for woofer systems can be applied to tweeters and other high-frequency drivers successfully. However, there are general differences in the large signal behavior between the two types of drivers:

The maximal output of most woofers is limited by relatively soft nonlinearities and the temperature of the voice coil. Hard clipping nonlinearities caused by voice coil hitting on the back plate or short wires are considered as defects. Contrary, most high-frequency drivers have no mechanical protection capabilities due to the lack of a regular suspension. High displacement may cause a permanent damage of the driver. The free coil movement, length and position of the wires and the way coils are glued on the diaphragm are critical.

Nevertheless the classical nonlinearities in motor and suspension may cause significant distortion. The examples presented in the paper and many other high-frequency drivers measured by the author before have dominant 2nd-order distortion corresponding to asymmetries in the stiffness and force factor characteristic. Applying finite element analysis (FEA) may reveal the geometrical causes.

The higher resonance frequency changes the spectral properties of motor and suspension distortion. While in woofers $K_{ms}(x)$ -distortion are restricted to low frequencies the spectrum of $K_{ms}(x)$ -distortion found in high-frequency drivers spreads to the middle of the audio band. Contrary to woofers where intermodulation components generated by $Bl(x)$ and $L_e(x)$ have a small distance to the high-frequency probe tone (< 100 Hz) causing a characteristic roughness of the sound, the intermodulation distortion in tweeters have a much higher distance to the fundamentals (1 kHz and more) and change the timbre of the sound. They may also be detected as separate disturbances.

Visco-elastic behavior plays also an important role in high-frequency drivers. Especially magneto-fluid in the gap and impregnated fabric in the diaphragm causes significant changes in the mechanical loss factor with amplitude and time. Most of those processes are reversible. During a long term test the mechanical damping decreases which produces more displacement and higher distortion at resonance than in a short measurement without prior excitation.

The measurement technique of equivalent input distortion is convenient for the evaluation of large signal performance of high-frequency drivers. Resonances in the acoustical environment do not appear in the distortion responses which makes it much simpler to interpret them. The distortion at any point in the sound field may be predicted by using the equivalent input distortion and the linear transfer function.

The large signal model using a few number of lumped parameters can not explain nonlinear mechanisms in the diaphragm closely related with the occurrence of partial vibrations at higher frequencies. Fortunately, in common tweeters and micro-speakers the break-up modes start at very high frequencies and the amplitude of the difference tones falling back to the audio band is relatively small. Only in horn compression drivers this may be a practical issue because diaphragms with relatively large diameters are used. Applying nonlinear FEA to common diaphragm and cones would be an interesting subject for further research.

8. REFERENCES

- [1] M. Gander, "Dynamic Linearity and Power Compression in Moving-Coil Loudspeakers," *J. Audio Eng. Soc.* vol. 34, pp. 895 - 904 (1986 November).
- [2] W. Klippel, "Measurement of Large-Signal Parameters of Electrodynamic Transducer," presented at the 107th Convention of the Audio Engineering Society, New York, September 24-27, 1999, preprint 5008.
- [3] A. J. Kaiser, "Modeling of the Nonlinear Response of an Electrodynamic Loudspeaker by a Volterra Series Expansion," *J. Audio Eng. Soc.* 35, p. 421, (1987 Juni).
- [4] W. Klippel, "Diagnosis and Remedy of Nonlinearities in Electro-dynamical Woofers," presented at the 109th Convention of the Audio Engineering Society, Los Angeles, September 22-25, 2000, preprint 5261
- [5] M. Dodd, et. al., "Voice Coil Impedance as a Function of Frequency and Displacement" presented at the 117th Convention of the Audio Eng. Soc. , 2004 October 28–31 San Francisco, CA, USA.
- [6] Henricksen, "Heat Transfer Mechanisms in Loudspeakers: Analysis, Measurement and Design," *J. Audio Eng. Soc.* Vol 35. No. 10 , 1987 October.
- [7] D. Button, Heat Dissipation and Power Compression in Loudspeakers, *J. Audio Eng. Soc.*, Vol. 40, No1/2 1992 January/February.
- [8] C. Zuccatti, Thermal Parameters and Power Ratings of Loudspeakers, *J. Audio Eng. Soc.*, Vol. 38, No. 1,2, 1990 January/February.
- [9] W. Klippel, "Nonlinear Modeling of the Heat Transfer in Loudspeakers," *J. Audio Eng. Society* **52**, 2004 January.
- [10] M. Dodd, "The Development of a Forward Radiating Compression Driver by the Application of Acoustic, Magnetic and Thermal Finite Element Methods," Presented at the 115th Convention of the Audio Engineering Society, preprint 5886, September 2003.
- [11] W. Klippel, "Equivalent Input Distortion," *J. Audio Eng. Society* **52**, No. 9 pp. 931-947 (2004 Sept.).
- [12] D. Clark, „Precision Measurement of Loudspeaker Parameters," *J. Audio Eng. Soc.* vol. 45, pp. 129 - 140 (1997 March).
- [13] M.H. Knudsen and J.G. Jensen, "Low-Frequency Loudspeaker Models that Include Suspension Creep," *J. Audio Eng. Soc.*, vol. 41, pp. 3-18, (Jan./Feb. 1993)
- [14] W. Klippel, "Distortion Analyzer – a New Tool for Assessing and Improving Electrodynamic Transducers,"

presented at the 108th Convention of the Audio Engineering Society, Paris, February 19-22, 2000, preprint 5109

[15] E. Czerwinski, et. al., "Multitone Testing of Sound System Components – Some Results and Conclusions, J. Audio Eng. Soc. vol. 49, pp. 1011 - 1048 (2001 Nov.).

[16] W. Klippel, "Assessment of Voice-Coil Peak Displacement X_{\max} ," J. Audio Eng. Society **51**, Heft 5, pp. 307 - 323 (2003 May).

[17] W. Klippel, "Prediction of Speaker Performance at High Amplitudes," presented at 111th Convention of the Audio Engineering Society, 2001 September 21–24, New York, NY, USA

[18] Specification of the KLIPPEL Analyzer module, Klippel GmbH, www.klippel.de, 2003.